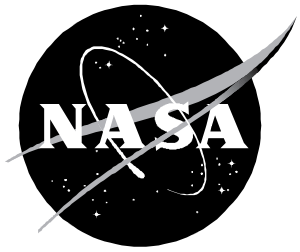

NASA Contractor Report 4764

Frequency Response Calculations of Input Characteristics of Cavity-Backed Aperture Antennas Using AWE With Hybrid FEM / MoM Technique

C. J. Reddy
Hampton University • Hampton, Virginia

M. D. Deshpande
ViGYAN, Inc. • Hampton, Virginia

National Aeronautics and Space Administration
Langley Research Center • Hampton, Virginia 23681-0001

Prepared for Langley Research Center
under Cooperative Agreement NCC1-231

February 1997

CONTENTS

	Abstract	2
	List of Symbols	3
1.0	Introduction	5
2.0	Hybrid FEM/MoM Technique	7
3.0	AWE Implementation	11
4.0	Numerical Results	12
5.0	Concluding Remarks	16
	Acknowledgments	17
	Appendix	18
	References	20

Abstract

Application of Asymptotic Waveform Evaluation (AWE) is presented in conjunction with a hybrid Finite Element Method (FEM) / Method of Moments (MoM) technique to calculate the input characteristics of cavity-backed aperture antennas over a frequency range. The hybrid FEM/ MoM technique is used to form an integro-partial-differential equation to compute the electric field distribution of the cavity-backed aperture antenna. The electric field, thus obtained, is expanded in a Taylor series around the frequency of interest. The coefficients of Taylor series (called “moments”) are obtained using the frequency derivatives of the integro-partial-differential equation formed by the hybrid FEM/MoM technique. Using the moments the electric field in the cavity is obtained over a frequency range. Using the electric field at different frequencies, the input characteristics of the antenna are obtained over a wide frequency band. Numerical results for an open coaxial line, probe fed cavity, and cavity-backed microstrip patch antennas are presented. Good agreement between AWE and the exact solution over the frequency range is observed.

List of Symbols

∇	Del operator
∇'	Del operator over the source coordinates
ε_r	Dielectric permittivity of the medium in the cavity
ε_{rc}	Dielectric permittivity of the medium in the coaxial feed line
δ_{qo}	Kronecker delta defined in equation (22)
μ_r	Dielectric permeability of the medium in the cavity
ρ	ρ-coordinate of the cylindrical coordinate system
$\hat{\rho}$	Unit normal vector along the ρ-axis
ω	Angular frequency
AWE	Asymptotic Waveform Evaluation
$A^{(q)}(k_o)$	qth derivative of $A(k)$ with respect to k; $\frac{d^q}{dk^q}A(k)$, evaluated at k_o
a_o	Reflection coefficient at the input plane S_{inp}
$b(k)$	Excitation vector
$b^{(q)}(k_o)$	qth derivative of $b(k)$ with respect to k; $\frac{d^q}{dk^q}b(k)$, evaluated at k_o
ds	Surface integration with respect to observation coordinates
ds'	Surface integration with respect to source coordinates
$\mathbf{E}$	Electric field
$\mathbf{E}_{inp}$	Electric field at the input plane S_{inp}
$e(k)$	Electric field coefficient vector
$\mathbf{e}_{inc}$	Incident electric field due to coaxial line at the surface S_{inp}
$\mathbf{e}_{ref}$	Reflected electric field into the coaxial line at the surface S_{inp}
$\mathbf{H}_{ap}$	Magnetic field at the surface S_{ap}

$\mathbf{H}_{inp}$	Magnetic field at the surface S_{inp}
f	Frequency
j	$\sqrt{-1}$
k	Wavenumber at any frequency f
k_o	Wavenumber at frequency f_o
$\mathbf{M}$	Magnetic current at the surface S_{ap}
M_n	nth moment of AWE ($n=0,1,2,3,4$ .....)
$\hat{\mathbf{n}}$	Normal unit vector
$q!$	Factorial of number q
R	Distance between the source point and the observation point
r_1	Radius of inner conductor of the coaxial feed line
r_2	Radius of outer conductor of the coaxial feed line
$\mathbf{T}$	Vector testing function
$\mathbf{T}_s$	Vector testing function at the surface S_{ap}
Y_{in}	Normalized input admittance of the antenna
$\mathbf{z}$	Unit normal along Z-axis

1. Introduction

Cavity-backed aperture antennas are very popular in aerospace applications due to their conformal nature. These antennas can be analyzed using the integral equation or differential equation methods. The integral equation approach involves the solution of a fully dense matrix equation and mathematically complex for inhomogeneous material and arbitrarily shaped cavities. The differential equation method can easily handle the arbitrarily shaped cavities with inhomogenous materials, but requires boundary truncation. Hybrid techniques have become attractive for numerical analysis of these type of problems due to their ability to handle arbitrary shape of the cavity and complex materials that may be required for the antenna design. The combined Finite Element Method (FEM) and Method of Moments (MoM) technique in particular has been used to analyze various cavity-backed aperture antennas[1,2]. In the combined FEM/MoM technique, FEM is used in the cavity volume to compute the electric field, whereas MoM is used to compute the magnetic current at the aperture. Using Galerkin's technique and forming simultaneous equations, the electric field is solved. For the combined FEM/MoM technique, the cavity is divided into tetrahedral elements and the aperture is discretized by triangles. Simultaneous equations are generated over the subdomains and are added to form a global matrix equation. This results in a partly sparse and partly dense symmetric complex matrix, which can be solved either by a direct solver or by an iterative solver. The electric field hence obtained is used to compute the radiation characteristics and input characteristics of the antenna.

In most practical applications, input characteristics such as input impedance or input admittance are of interest over a frequency range. To obtain the frequency response of the antenna, one has to repeat the above calculations at every incremental frequency over the frequency band of interest. If the antenna is highly frequency dependent, one needs to do the

calculations at fine increments of frequency to get an accurate representation of the frequency response. This can be computationally intensive for electrically large cavity with a large aperture and in some cases computationally prohibitive. To alleviate the above problems, the application of Asymptotic Waveform Evaluation (AWE) [3] to the combined FEM/MoM technique is proposed. Recently a detailed description of AWE was applied to frequency domain electromagnetic analysis and is presented in [4]. AWE has also been used to predict radar cross section (RCS) of perfect electric conductor (PEC) bodies over a frequency range [5].

In this report, we describe the application of AWE for calculating the input characteristics of a cavity-backed aperture antenna over a band of frequencies using the combined FEM/MoM technique. In the AWE technique, the electric field is expanded in Taylor's series around a frequency. The coefficients of Taylor series (called 'moments') are evaluated using the frequency derivatives of the combined FEM/MoM equation. Once the moments are obtained, the electric field distribution in the cavity can be obtained at any frequency over the frequency range. Using this field distribution, the input characteristics of the cavity-backed aperture antenna are obtained.

The rest of the report is organized as described below. In section 2, the combined FEM/MoM formulation is presented. In section 3, AWE implementation for the combined FEM/MoM technique is described. Numerical results for an open coaxial line, a coaxial cavity, and a cavity-backed microstrip patch antenna are presented in section 4. The numerical data are compared with the exact solution over the bandwidth. CPU time and storage requirements for AWE formulation are given for each example and are compared with those required for exact solution at each frequency. Concluding remarks on the advantages and disadvantages of the AWE technique are presented in section 5.

2. Combined FEM/MoM Technique for Cavity-Backed Aperture Antennas in Infinite Ground Plane

The geometry of the problem to be analyzed is shown in figure 1. For linear, isotropic, and source free region; the electric field satisfies the vector wave equation:

$$\nabla\times\left(\frac{1}{\mu_r}\nabla\times\mathbf{E}\right)-k^2\varepsilon_r\mathbf{E}\;=\;0 \tag{1}$$

where μ_r, ε_r are the relative permeability and relative permittivity of the medium in the cavity. The time variation $\exp(j\omega t)$ is assumed and suppressed throughout this report. Applying the Galerkin's technique, equation (1) can be written in "weak form" as [6]

$$\iiint_V (\nabla\times\mathbf{T})\bullet\left(\frac{1}{\mu_r}\nabla\times\mathbf{E}\right)dv-k^2\varepsilon_r\iiint_V\mathbf{T}\bullet\mathbf{E}\,dv-j\omega\mu_o\iint_{S_{ap}}(\mathbf{T}\times\hat{\mathbf{n}})\bullet\mathbf{H}_{ap}\,ds$$

$$=\quad j\omega\mu_o\iint_{S_{inp}}\mathbf{T}\bullet(\hat{\mathbf{n}}\times\mathbf{H}_{inp})\,ds \tag{2}$$

where $\mathbf{T}$ is the vector testing function, S_{ap} is the aperture surface, and S_{inp} is the input surface (see figure 1). $\mathbf{H}_{ap}$ is the magnetic field at the aperture and $\mathbf{H}_{inp}$ is the magnetic field at the input surface.

In accordance with the equivalence principle [7], the fields inside the cavity can be decoupled to the fields outside the cavity by closing the aperture with a PEC and introducing the equivalent magnetic current.

$$\mathbf{M}\;=\;\mathbf{E}\times\hat{\mathbf{z}} \tag{3}$$

over the extent of the aperture. Making use of the image theory, the integrals over S_{ap} in equation (2) can be written as

$$j\omega\mu_o \iint_{S_{ap}} (\mathbf{T}\times\hat{\mathbf{n}}) \bullet \mathbf{H}_{ap} ds$$

$$= \frac{k^2}{2\pi} \iint_{S_{ap}} \mathbf{T}_s \bullet \left(\iint_{S_{ap}} \mathbf{M} \frac{\exp(-jkR)}{R} ds' \right) ds$$

$$- \frac{1}{2\pi} \iint_{S_{ap}} (\nabla \bullet \mathbf{T}_s) \left\{ \iint_{S_{ap}} (\nabla' \bullet \mathbf{M}) \frac{\exp(-jkR)}{R} ds' \right\} ds \qquad (4)$$

where $\mathbf{T}_s = \mathbf{T}\times\hat{\mathbf{n}}$ and R is the distance between source point and the observation point. ∇' indicates del operation over the source coordinates and ds' indicates the surface integration over the source region.

Though the analysis presented in this report is not restricted to any specific input feed structure, we restrict the presentation of the formulation to the coaxial line as the input feed structure. The cross section of the coaxial line is shown in figure 2. Assuming that the incident electric field is the dominant transverse electric and magnetic (TEM) mode and the reflected field also consists of TEM mode only, the electric field at the input plane S_{inp} is given by

$$\mathbf{E}_{inp} = \mathbf{e}_{inc} \exp\left(-jk\sqrt{\varepsilon_{rc}}z\right) + \mathbf{e}_{ref} \exp\left(jk\sqrt{\varepsilon_{rc}}z\right) \qquad (5)$$

where

$$\mathbf{e}_{inc} = \hat{\rho} \frac{1}{\sqrt{2\pi \ln\left(\frac{r_2}{r_1}\right)}} \frac{1}{\rho} \qquad (6)$$

and

$$\mathbf{e}_{ref} = a_o \mathbf{e}_{inc} \qquad (7)$$

a_o is the reflection coefficient and is given by

$$a_o = \frac{\exp\left(-jk\sqrt{\varepsilon_{rc}}z_1\right)}{\sqrt{2\pi\ln\left(\frac{r_2}{r_1}\right)}}\int\int_{S_{inp}} \mathbf{E}\bullet\left(\frac{\hat{\rho}}{\rho}\right)ds - \exp\left(-2jk\sqrt{\varepsilon_{rc}}z_1\right) \tag{8}$$

r_2 is the outer radius and r_1 is the inner radius of the coaxial line. ε_{rc} is the relative permittivity of the coaxial line.

Using equation (5) to calculate $\mathbf{H}_{inp}$, the surface integral over S_{inp} in equation (2) can be written as

$$j\omega\mu_o\int\int_{S_{inp}} \mathbf{T}\bullet(\hat{\mathbf{n}}\times\mathbf{H}_{inp})\,ds$$

$$= \frac{-jk\sqrt{\varepsilon_{rc}}}{2\pi\ln\left(\frac{r_2}{r_1}\right)\mu_{rc}}\left\{\int\int_{S_{inp}} \mathbf{T}\bullet\left(\frac{\hat{\rho}}{\rho}\right)ds\right\}\left\{\int\int_{S_{inp}} \mathbf{E}\bullet\left(\frac{\hat{\rho}}{\rho}\right)ds\right\}$$

$$+ \frac{2jk\sqrt{\varepsilon_{rc}}\exp\left(-jk\sqrt{\varepsilon_{rc}}z_1\right)}{\mu_{rc}\sqrt{2\pi\ln\left(\frac{r_2}{r_1}\right)}}\int\int_{S_{inp}} \mathbf{T}\bullet\left(\frac{\hat{\rho}}{\rho}\right)ds \tag{9}$$

Substituting equation (4) and (8) in equation (2), the system equations for the combined FEM/ MoM technique can be written as

$$\iiint_V \frac{1}{\mu_r}(\nabla\times\mathbf{T})\bullet(\nabla\times\mathbf{E})\,dv - k^2\varepsilon_r\iiint_V \mathbf{T}\bullet\mathbf{E}\,dv$$

$$-\frac{k^2}{2\pi}\int\int_{S_{ap}} \mathbf{T}_s\bullet\left(\int\int_{S_{ap}} \mathbf{M}\frac{\exp(-jkR)}{R}ds'\right)ds + \frac{1}{2\pi}\int\int_{S_{ap}}(\nabla\bullet\mathbf{T}_s)\left\{\int\int_{S_{ap}}(\nabla'\bullet\mathbf{M})\frac{\exp(-jkR)}{R}ds'\right\}ds$$

$$+ \frac{jk\sqrt{\varepsilon_{rc}}}{2\pi\ln\left(\frac{r_2}{r_1}\right)\mu_{rc}}\left\{\int\int_{S_{inp}} \mathbf{T}\bullet\left(\frac{\hat{\rho}}{\rho}\right)ds\right\}\left\{\int\int_{S_{inp}} \mathbf{E}\bullet\left(\frac{\hat{\rho}}{\rho}\right)ds\right\}$$

$$= \frac{2jk\sqrt{\varepsilon_{rc}}\exp\left(-jk\sqrt{\varepsilon_{rc}}z_1\right)}{\mu_{rc}\sqrt{2\pi\ln\left(\frac{r_2}{r_1}\right)}}\int\int_{S_{inp}} \mathbf{T}\bullet\left(\frac{\hat{\rho}}{\rho}\right)ds \qquad (10)$$

The volume of the cavity is subdivided into small volume tetrahedral elements. The electric field is expressed in terms of the edge vector basis functions [6], which enforce the divergenceless condition of the electric field explicitly. The vector testing function is also expressed in terms of the edge vector basis functions following the Galerkin's method. The discretization of the cavity volume into tetrahedral elements automatically results in discretization of the surfaces S_{ap} and S_{inp} into triangular elements. The volume and surface integrals in equation (10) are carried out over each element to form element matrices and the element matrices are assembled to form global matrices. Equation (10) can be written in matrix form as

$$A(k)\,e(k) = b(k) \qquad (11)$$

$A(k)$ is a partly sparse, partly dense complex symmetric matrix, *b(k)* is the excitation vector, and *e(k)* is the unknown electric field coefficient vector. *A(k)* is evaluated as a sum of three matrices.

$$A(k) = A_1(k) + A_2(k) + A_3(k) + A_4(k) \qquad (12)$$

where

$$A_1(k) = \iiint_V \frac{1}{\mu_r}(\nabla\times\mathbf{T})\bullet(\nabla\times\mathbf{E})\,dv - k^2\varepsilon_r\iiint_V \mathbf{T}\bullet\mathbf{E}\,dv \qquad (13)$$

$$A_2(k) = -\frac{k^2}{2\pi}\int\int_{S_{ap}} \mathbf{T}_s\bullet\left(\int\int_{S_{ap}} \mathbf{M}\frac{\exp(-jkR)}{R}ds'\right)ds \qquad (14)$$

$$A_3(k) = \frac{1}{2\pi}\int\int_{S_{ap}} (\nabla\bullet\mathbf{T}_s)\left\{\int\int_{S_{ap}} (\nabla'\bullet\mathbf{M})\frac{\exp(-jkR)}{R}ds'\right\}ds \qquad (15)$$

$$A_4(k) = \frac{jk\sqrt{\varepsilon_{rc}}}{2\pi \ln\left(\frac{r_2}{r_1}\right)\mu_{rc}} \left\{ \int\int_{S_{inp}} \mathbf{T} \bullet \left(\frac{\hat{\rho}}{\rho}\right) ds \right\} \left\{ \int\int_{S_{inp}} \mathbf{E} \bullet \left(\frac{\hat{\rho}}{\rho}\right) ds \right\} \tag{16}$$

$$b(k) = \frac{2jk\sqrt{\varepsilon_{rc}} \exp\left(-jk\sqrt{\varepsilon_{rc}} z_1\right)}{\mu_{rc}\sqrt{2\pi \ln\left(\frac{r_2}{r_1}\right)}} \int\int_{S_{inp}} \mathbf{T} \bullet \left(\frac{\hat{\rho}}{\rho}\right) ds \tag{17}$$

The matrix equation (11) is solved at any specific frequency, f_o (with wavenumber k_o) either by a direct method or by an iterative method. The solution of the equation (11) gives the unknown electric field coefficients which are used to obtain the electric field distribution. Once the electric field distribution is known, the input reflection coefficient can be calculated using equation (8). The input plane is placed at $z_1 = 0$, and the reflection coefficient is calculated as

$$\Gamma = a_o\big|_{z_1 = 0} = \frac{1}{\sqrt{2\pi \ln\left(\frac{r_2}{r_1}\right)}} \int\int_{S_{inp}} \mathbf{E} \bullet \left(\frac{\hat{\rho}}{\rho}\right) ds - 1 \tag{18}$$

The normalized input admittance at S_{inp} is given by

$$Y_{in} = \frac{1 - \Gamma}{1 + \Gamma} \tag{19}$$

The input admittance given in equation (18) is calculated at one frequency. If one needs the input admittance over a frequency range, this calculation is to be repeated at different frequency values.

3. AWE Implementation

The general implementation of AWE for any frequency domain technique used for electromagnetic analysis is given in detail in [4]. As shown in the previous section, the solution of equation (11) gives the unknown electric field coefficient vector $e(k_o)$ at a particular frequency f_o. However at any k, $e(k)$ can be expanded in Taylor series as

$$e(k) = \sum_{n=0}^{\infty} M_n (k - k_o)^n \tag{20}$$

with the moments M_n given by [4]

$$M_n = A^{-1}(k_o)\left[\frac{b^{(n)}(k_o)}{n!} - \sum_{q=0}^{n} \frac{(1-\delta_{qo})A^{(q)}(k_o)M_{n-q}}{q!}\right] \tag{21}$$

$A^{(q)}(k_o)$ is the *q*th derivative with respect to *k* of *A(k)* given in equation (12) and evaluated at k_o. Similarly, $b^{(q)}(k_o)$ is the *q*th derivative with respect to *k* of *b(k)* given in equation (16) and evaluated at k_o. The Kronecker delta δ_{qo} is defined as

$$\delta_{qo} = \begin{cases} 1 & q = 0 \\ 0 & q \neq 0 \end{cases} \tag{22}$$

The q*th* derivatives of *A(k)* and *b(k)* are evaluated and are given in detail in the Appendix.

Once the moments of AWE are obtained, the electric field coefficients at frequencies around the expansion frequency are obtained by using the equation (20). The electric field hence obtained is used to compute the input characteristics of the cavity-backed aperture antenna over a frequency range.

4. Numerical Results

To validate the analysis presented in the previous sections, a few numerical examples are considered. Input characteristic calculations over a frequency range are done for an open coaxial line, coaxial cavity, and cavity-backed square and circular microstrip patch antennas. The numerical data obtained using AWE are compared with the results calculated at each frequency using the computer code CBS3DR[9], which implements the combined FEM/MoM technique[2]. We will refer to the latter method as “exact solution”. From section 3, it can be observed that the

inverse of matrix $A(k_o)$ is found once and is used repeatedly to find AWE moments. Due to the hybrid FEM/MoM technique, matrix $A(k_o)$ is partly sparse and partly dense. The Complex Vector Sparse Solver (CVSS) [10] is used to LU factor the matrix $A(k_o)$ once and the moments are obtained by backsolving the equation (21) with multiple righthand sides. All the computations reported below are done on a CONVEX C-220 computer.

(a) Open Coaxial line:

An open coaixial line radiating into an infinite ground plane (fig. 3a) is considered. A finite length of the line is used for FEM discretization. The input plane S_{inp} is placed at $z = 0$ plane and the radiating aperture at $z = 1cm$. The discretization of the coaxial line resulted in 1119 total unknowns, and the order of the dense matrix due to MoM is 144. The frequency response of the input admittance is calculated with 6 GHz as the expansion frequency. The AWE moments are calculated at 6 GHz and are used in the Taylor series expansion. The frequency response from 4 GHz to 8 GHz is plotted in figure 3(b) along with the exact solution calculated at different frequencies. A good trend in frequency response is predicted by the 2nd order AWE[1], whereas a very good agreement can be seen between the 5th order AWE frequency response and the exact solution over the frequency range. The 1119X1119 hybrid FEM/MoM matrix exact solution took around 150.7 secs of CPU time to fill the matrix and 10 secs to LU factor the matrix at each frequency. The 5th order AWE frequency response calculation took 328 secs of CPU time to fill the matrices including the frequency derivative matrices and 10 secs to LU factor the $A(k_o)$ matrix. The exact solution was carried out at nine frequency points with (160.7X9) 1446.30 secs of total CPU time. With AWE, the frequency response was calculated with 0.1 GHz frequency increments. It can be seen that there is a substantial amount of savings in CPU time by

1. As AWE is a purely mathematical approximation to the solution, it is observed that at some frequencies, 2nd order AWE results in unrealistic values of conductance.

using AWE, when frequency response of input characteristics are required with fine frequency increments.

(b) Open Coaxial Cavity:

An open coaxial cavity fed by a 50Ω coaxial line (fig. 4) is considered as a second example. The input plane S_{inp} is placed at $z = 0$ plane and the radiating aperture at $z = 0.952cm$ plane. The cavity volume is discretized using tetrahedral elements, which resulted in 4541 total unknowns and the order of the dense matrix due to MoM is 666. The frequency response of the return loss ($=20\log|\Gamma|$) is calculated with 6 GHz as the expansion frequency. The AWE moments are calculated at 6 GHz and are used in the Taylor series expansion. The frequency response from 5 GHz to 7 GHz is plotted in figure 5 along with the exact solution calculated at different frequencies. It can be seen from figure 5 that 2nd order AWE could not predict the frequency response over the frequency range, whereas a very good agreement can be seen between the 5th order AWE frequency response and the exact solution over the frequency range. The 4541X4541 hybrid FEM/MoM matrix exact solution took around 2027 secs of CPU time to fill the matrix and 264 secs to LU factor the matrix at each frequency. The 5th order AWE frequency response calculation took 4867 secs of CPU time to fill the matrices including the frequency derivative matrices and 264 secs to LU factor the $A(k_o)$ matrix. The exact solution was carried out at nine frequency points with (2,291X9) 20,619 secs of total CPU time. With AWE the frequency response was calculated with 0.1 GHz frequency increments with 5,140 secs of total CPU time.

(c) Cavity-Backed Square Microstrip Patch Antenna:

A cavity-backed square microstrip antenna radiating into an infinite ground plane (fig. 6) is considered. The input plane S_{inp} is placed at $z = 0$ plane and the radiating aperture at

$z = 0.16cm$. The discretization of the cavity volume resulted in 2,160 total unknowns and the order of the dense matrix due to MoM is 544. The frequency response of the input impedance $(1/Y_{in})$ is calculated with 4 GHz as the expansion frequency. The AWE moments are calculated at 4GHz and are used in the Taylor series expansion. To obtain an accurate frequency response over a wider frequency range, another set of moments are calculated at 4.3 GHz. The frequency response from 3.8 GHz to 4.5 GHz is plotted in figure 7 along with the exact solution calculated at different frequencies. A very good agreement can be seen between the 5th order AWE frequency response and the exact solution over the frequency range. The 2160X2160 hybrid FEM/MoM matrix exact solution took around 1558secs of CPU time to fill the matrix and 122secs to LU factor the matrix at each frequency. The 5th order AWE frequency response calculation took 3754 secs of CPU time to fill the matrices including the frequency derivative matrices and 122 secs to LU factor the $A(k_o)$ matrix. The exact solution was carried out at nine frequency points with (1,680X9) 15,120 secs of total CPU time. With two expansion points, AWE took 7,752s ecs of total CPU time. With AWE the frequency response was calculated with 0.01 GHz frequency increments.

(d) Cavity-Backed Circular Microstrip Patch Antenna:

A cavity-backed circular microstrip antenna radiating into an infinite ground plane is shown in figure 8. The input plane S_{inp} is placed at $z = 0$ plane and the radiating aperture at $z = 0.16cm$. The discretization of the cavity volume resulted in 6,363 total unknowns and the order of the dense matrix due to MoM is 469. The frequency response of the input impedance $(1/Y_{in})$ is calculated with 6 GHz as the expansion frequency. The AWE moments are calculated at 6 GHz and are used in the Taylor series expansion. To obtain an accurate frequency response over a wider frequency range, another set of moments are calculated at 5.8 GHz. The frequency

response from 5.6 GHz to 6.2 GHz is plotted in figure 9 along with the exact solution calculated at different frequencies. A very good agreement can be seen between the 5th order AWE frequency response and the exact solution over the frequency range. The 6,363X6,363 hybrid FEM/MoM matrix exact solution took around 1,250 secs of CPU time to fill the matrix and 112secs to LU factor the matrix at each frequency. The 5th order AWE frequency response calculation took 2,967 secs of CPU time to fill the matrices including the frequency derivative matrices and 112 secs to LU factor the $A(k_o)$ matrix. The exact solution was carried out at seven frequency points with (1362X7) 9,534 secs of total CPU time. With two expansion points, AWE took 6,178secs of total CPU time. With AWE the frequency response was calculated with 0.01 GHz frequency increments. Considering the fact that with AWE around 60 frequency calculations could be carried out with less CPU time compared to calculate 7 frequency points with exact solution, AWE has a distinct advantage and is essential if one has to determine the exact resonant frequency.

5. Concluding Remarks

The AWE technique is applied to the hybrid FEM/MoM technique to obtain the frequency response of the input characteristics of cavity-backed aperture antennas. The frequency response of input characteristics of an open coaxial line, coaxial cavity, square microstrip patch anetnna, and a circular patch antenna are computed and compared with the exact solution. From the numerical examples presented in this work, AWE is found to be superior in terms of CPU time to obtain a frequency response. It may be noted that although calculations are done in frequency increments of 0.1 GHz or 0.01 GHz for the examples presented, the frequency response at even finer freqeuncy increments can also be calculated with a very nominal cost. The application of

AWE to three dimensional cavity-backed aperture antennas (without the infinite ground plane) is of interest for future research. The accuracy of AWE over a desired frequency band and its relation to the order of AWE to be used are also of interest for future research. With all of these topics addressed, AWE will be a good computing tool for the design of cavity-backed aperture antennas.

Acknowledgements

The authors would like to thank Dr. Olaf Storaasli of NASA Langley and Dr. Majdi Baddourah of National Energy Research Scientific Computing (NERSC) Center for providing the Complex Vector Sparse Solver (CVSS).

Appendix

Derivatives of *A(k)* and *b(k)* w.r.t. *k*

The frequency derivatives of *A(k)* and *b(k)* are evaluated and are given below. From equation (12):

$$A^{(q)}(k) = \frac{d^q A(k)}{dk^q} = A_1^{(q)}(k) + A_2^{(q)}(k) + A_3^{(q)}(k) + A_4^{(q)}(k) \quad q=0,1,2,3,..... \qquad (A.1)$$

From equation (13)

$$A_1^{(0)}(k) = \iiint_V \frac{1}{\mu_r}(\nabla\times\mathbf{T}) \bullet (\nabla\times\mathbf{E})\, dv - k^2\varepsilon_r \iiint_V \mathbf{T}\bullet\mathbf{E}\, dv \qquad (A.2)$$

$$A_1^{(1)}(k) = -2k\varepsilon_r \iiint_V \mathbf{T}\bullet\mathbf{E}\, dv \qquad (A.3)$$

$$A_1^{(2)}(k) = -2\varepsilon_r \iiint_V \mathbf{T}\bullet\mathbf{E}\, dv \qquad (A.4)$$

$$A_1^{(q)}(k) = 0 \qquad q \geq 3 \qquad (A.5)$$

From equation (14)

$$A_2^{(0)}(k) = -\frac{k^2}{2\pi} \iint_{S_{ap}} \mathbf{T}_s \bullet \left(\iint_{S_{ap}} \mathbf{M} \frac{\exp(-jkR)}{R} ds' \right) ds \qquad (A.6)$$

$$A_2^{(1)}(k) = \iint_{S_{ap}} \mathbf{T}_s \bullet \left(\iint_{S_{ap}} \mathbf{M}\left(\frac{j}{2\pi}\right) \left[2k + k^2(-jR)\right] \frac{\exp(-jkR)}{(-jR)} ds' \right) ds \qquad (A.7)$$

$$A_2^{(q)}(k) = \iint_{S_{ap}} \mathbf{T}_s \bullet \left(\iint_{S_{ap}} \mathbf{M}\left(\frac{j}{2\pi}\right) \left[\frac{q!}{(q-2)!}(-jR)^{q-3} + 2qk(-jR)^{q-2} + k^2(-jR)^{q-1} \right] \exp(-jkR)\, ds' \right) ds \quad \text{for } q>1 \qquad (A.8)$$

From equation (16)

$$A_3^{(0)}(k) = \frac{1}{2\pi}\int\int_{S_{ap}} (\nabla \bullet \mathbf{T}_s) \left\{ \int\int_{S_{ap}} (\nabla' \bullet \mathbf{M}) \frac{\exp(-jkR)}{R} ds' \right\} ds \tag{A.9}$$

$$A_3^{(q)}(k) = \int\int_{S_{ap}} (\nabla \bullet \mathbf{T}_s) \{ \int\int_{S_{ap}} (\nabla' \bullet \mathbf{M}) \left(-\frac{j}{2\pi} \right) (-jR)^{(q-1)} \exp(-jkR)\, ds' \}\, ds \tag{A.10}$$

From equation (17)

$$A_4^{(0)}(k) = \frac{jk\sqrt{\varepsilon_{rc}}}{2\pi \ln\left(\frac{r_2}{r_1}\right)\mu_{rc}} \left\{ \int\int_{S_{inp}} \mathbf{T} \bullet \left(\frac{\hat{\rho}}{\rho} \right) ds \right\} \left\{ \int\int_{S_{inp}} \mathbf{E} \bullet \left(\frac{\hat{\rho}}{\rho} \right) ds \right\} \tag{A.11}$$

$$A_4^{(1)}(k) = \frac{A_4^{(0)}(k)}{k} \tag{A.12}$$

$$A_4^{(q)}(k) = 0 \qquad q \geq 2 \tag{A.13}$$

From equation (18)

$$b^{(0)}(k) = \frac{2jk\sqrt{\varepsilon_{rc}} \exp\left(-jk\sqrt{\varepsilon_{rc}} z_1\right)}{\mu_{rc}\sqrt{2\pi \ln\left(\frac{r_2}{r_1}\right)}} \int\int_{S_{inp}} \mathbf{T} \bullet \left(\frac{\hat{\rho}}{\rho} \right) ds \tag{A.14}$$

$$b^{(q)}(k) = \left(-j\sqrt{\varepsilon_{rc}} z_1 \right)^q \left[1 - \frac{q}{jk\sqrt{\varepsilon_{rc}} z_1} \right] b^{(0)}(k) \tag{A.15}$$

Equation (A.15) is written in a compact form, however, it must be simplfied before evaluating at $z_1 = 0$.

References

[1] J. M. Jin and J. L. Volakis, "A hybrid finite element method for scattering and radiation by microstrip patch antennas and arrays residing in a cavity," *IEEE Trans. Antennas and Propagation*, Vol.39, pp.1598-1604, November 1991.

[2] C. J. Reddy, M. D. Deshpande, C. R. Cockrell and F. B. Beck, "Radiation characteristics of cavity backed aperture antennas in finite ground plane using the hybrid FEM/MoM technique and geometrical theory of diffraction," *IEEE Trans. Antennas and Propagation*, Vol.44, pp.1327-1333, October 1996.

[3] E. Chiprout and M. S. Nakhla, *Asymptotic Waveform Evaluation*, Kulwar Academic Publishers, 1994.

[4] C.R.Cockrell and F.B.Beck, "Asymptotic Waveform Evaluation (AWE) technique for frequency domain electromagnetic analysis," *NASA Technical Memorandum 110292*, November 1996.

[5] C. J. Reddy and M. D. Deshpande, "Application of AWE for RCS frequency response calculations using Method of Moments," *NASA Contractor Report 4758*, October 1996.

[6] C. J. Reddy, M. D. Deshpande, C. R. Cockrell and F. B. Beck, "Analysis of three-dimensional-cavity-backed aperture antennas using a combined finite element method/method of moments/geometrical theory of diffraction technique," *NASA Technical Paper 3548*, November 1995.

[7] R.F.Harrington, *Time Harmonic Electromagnetic Fields*, McGraw Hill Inc, 1961.

[8] S.M.Rao, D.R.Wilton and A.W.Glisson, "Electromagnetic scattering by surfaces of arbitrary shape," *IEEE Trans. Antennas and Propagation*, Vol.AP-30, pp.409-418, May 1982.

[9] C.J.Reddy and M.D.Deshpande, “User’s Manual for CBS3DR-Version 1.0,” *NASA Contractor Report 198284,* February 1996.

[10]O. O. Storaasli, “Performance of NASA equation solvers on computational mechanics applications ,” *American Institute of Aeronautics and Astronautics (AIAA) Paper No. 96-1505*, April, 1996

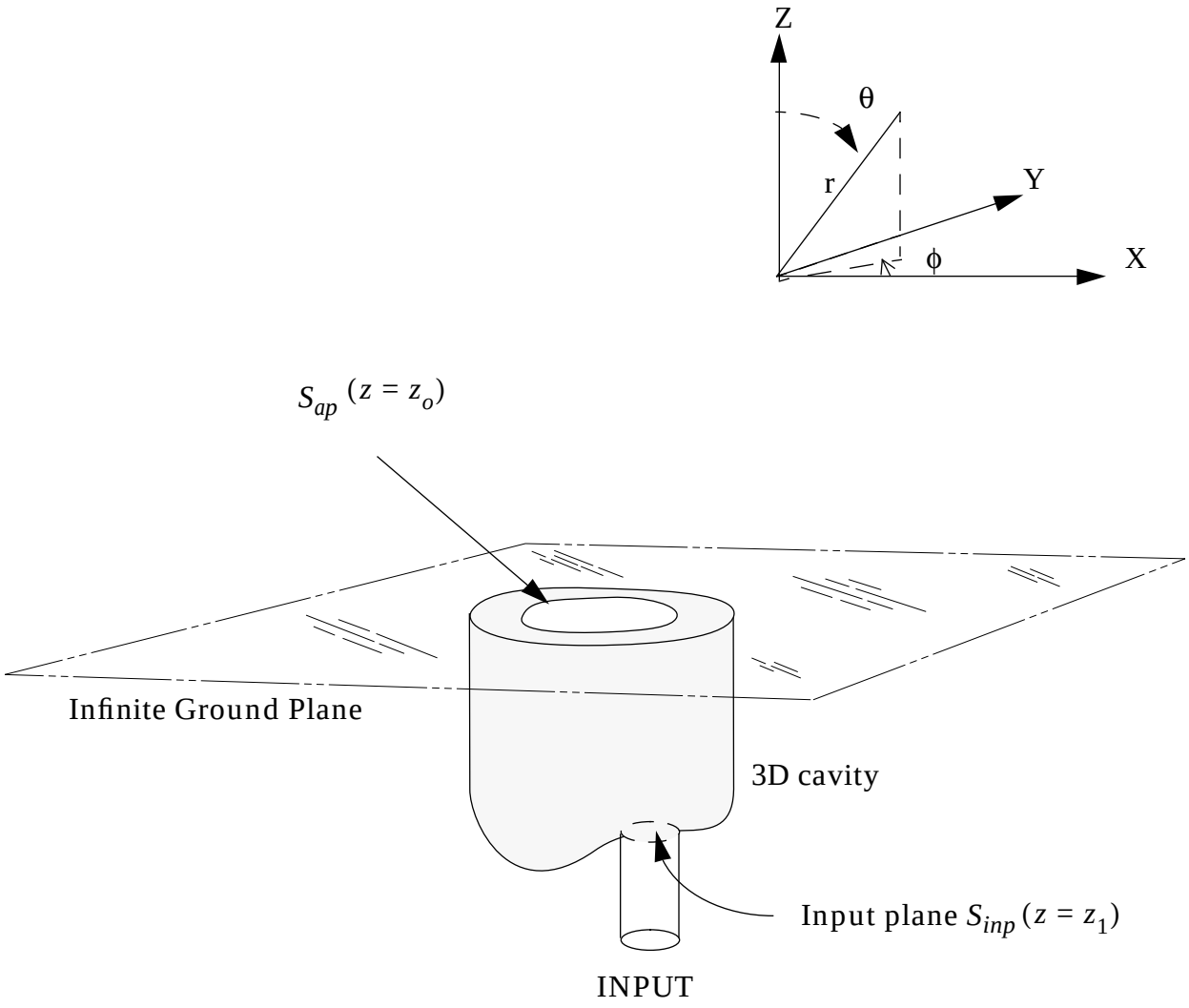

Figure 1 Geometry of a cavity backed aperture in finite ground plane.

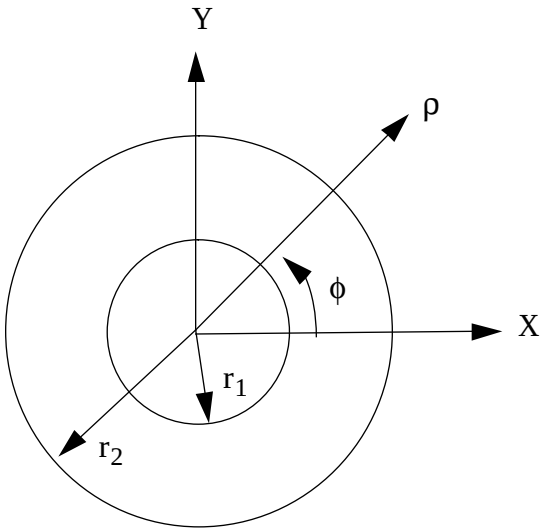

Figure 2 Cross section of the coaxial line.

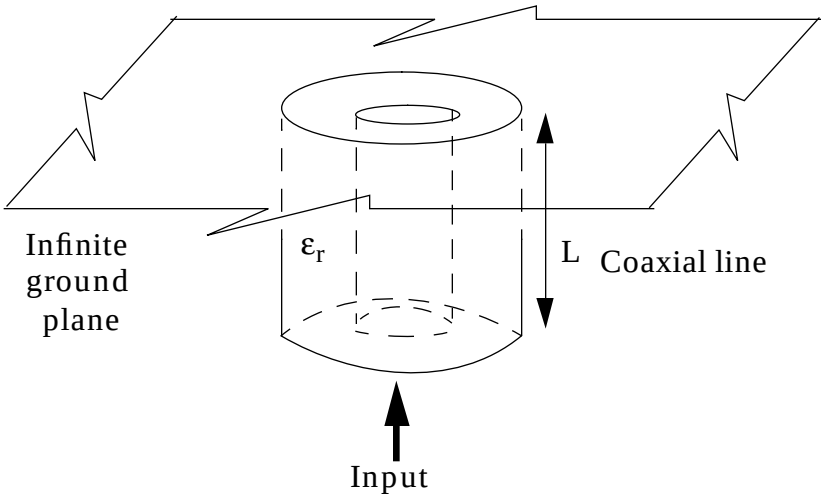

(a)

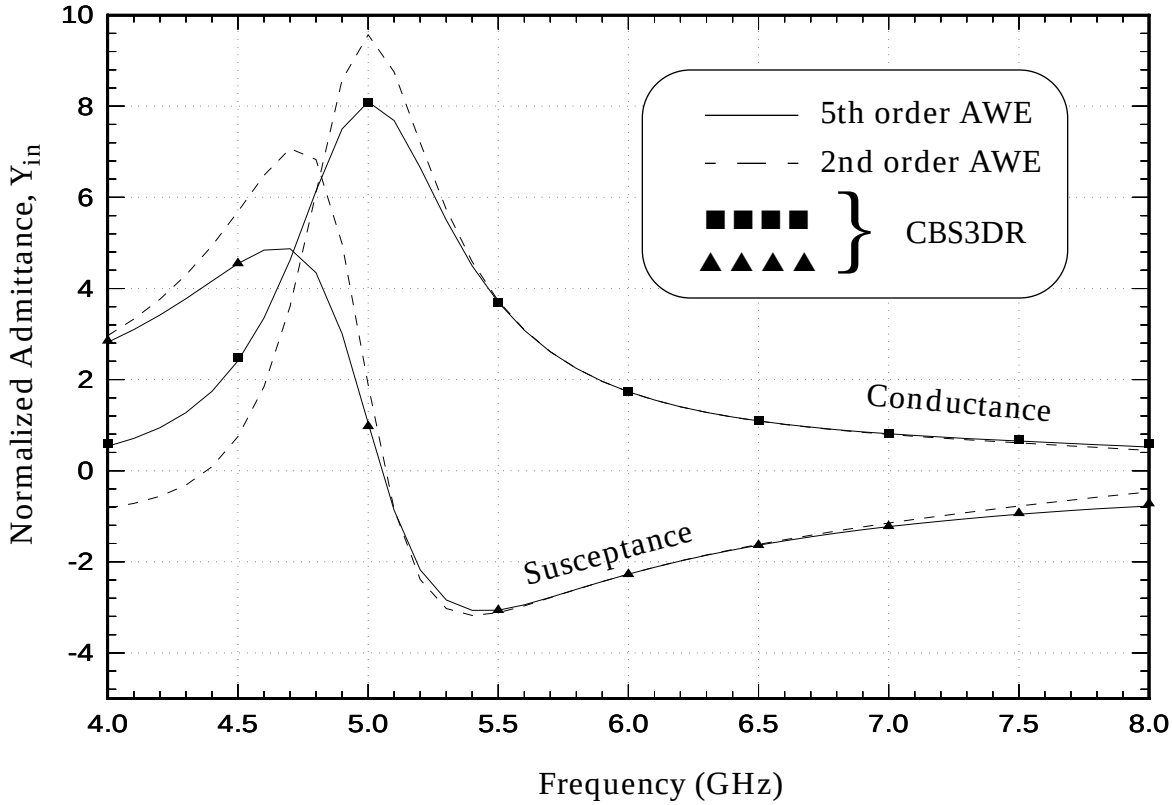

(b)

Figure 3 (a) Open coaxial line in an infinite ground plane. Inner radius r_1=1cm, Outer radius r_2=1.57cm, ε_r =1.0 and L=1.0cm
(b) Normalized input admittance as a function of frequency.

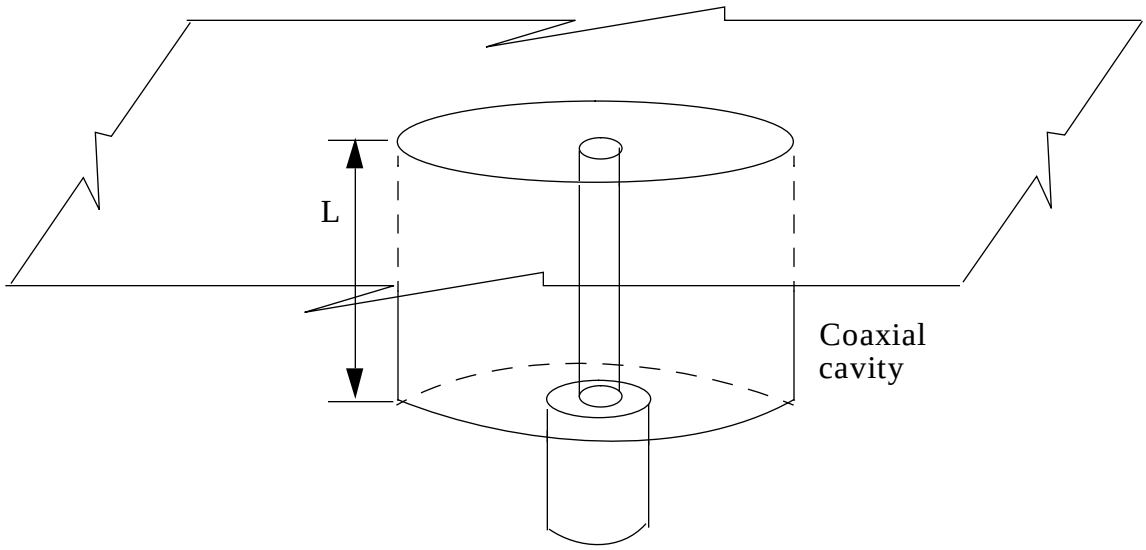

Figure 4 Geometry of a coaxial cavity in an infinite ground plane. Outer radius of the coaxial cavity=1", Inner radius of the coaxial cavity=0.0181" and L=3/8". The cavity is fed by a 50Ω coaxial line.

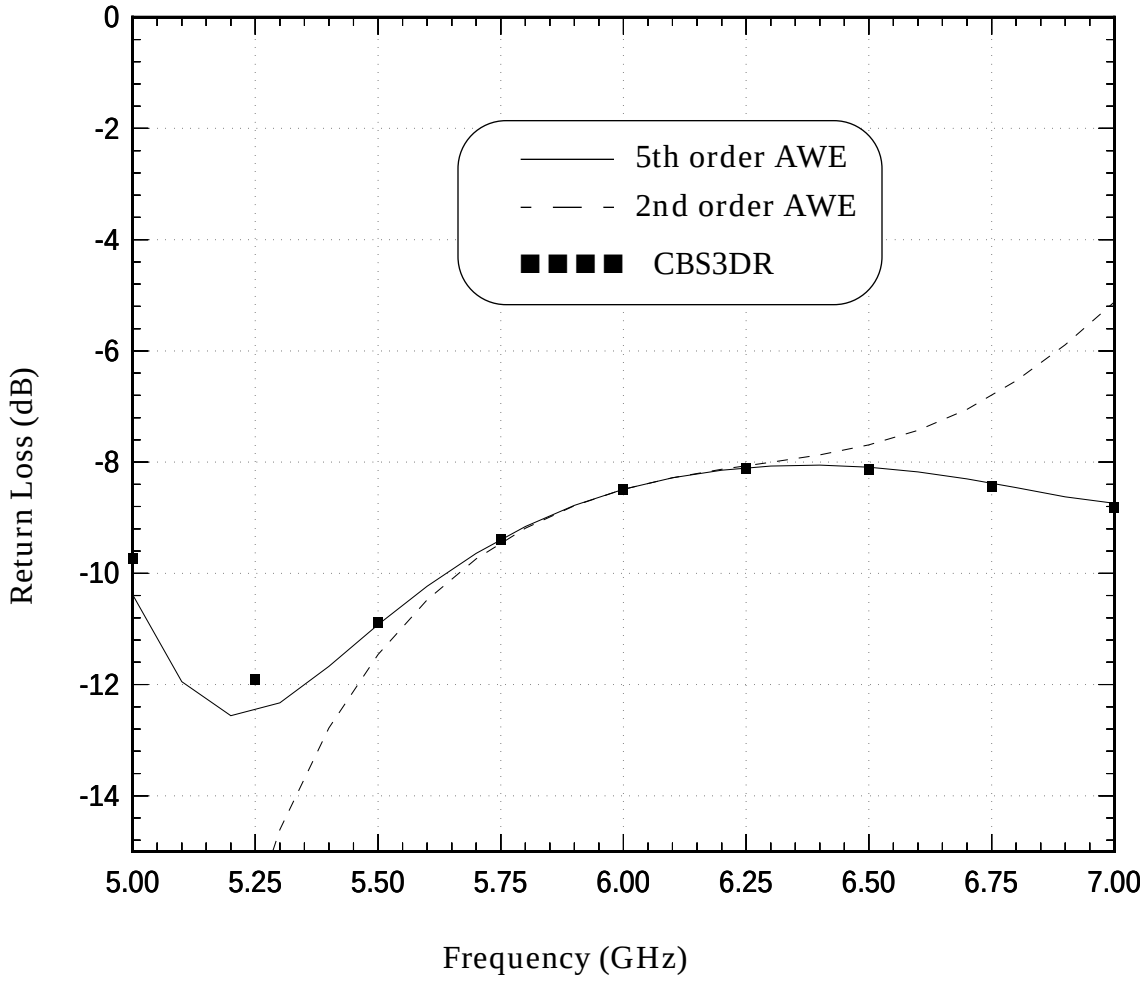

Figure 5 Return loss versus frequency of the coaxial cavity (figure 4).

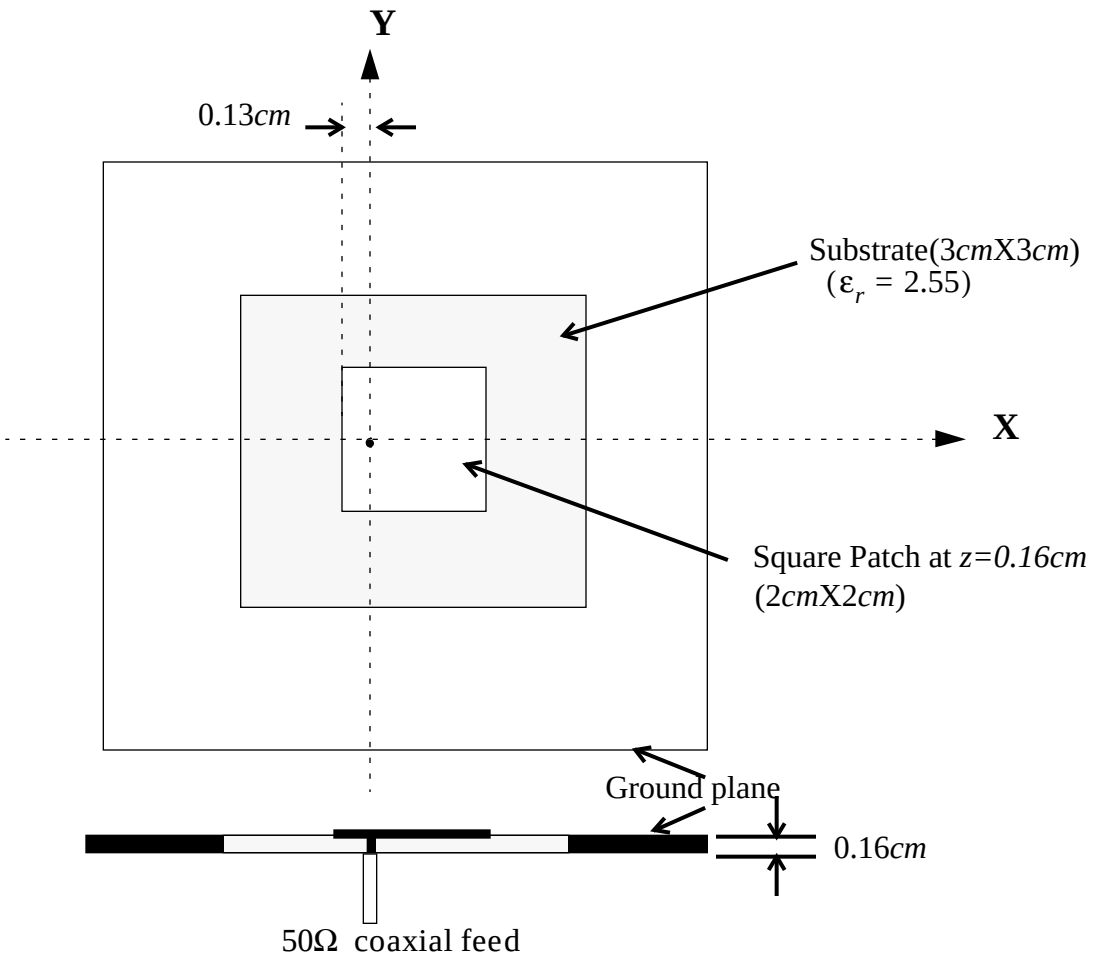

Figure 6 Cavity-backed square microstrip patch antenna in an infinite ground plane fed by a 50Ω coaxial line.

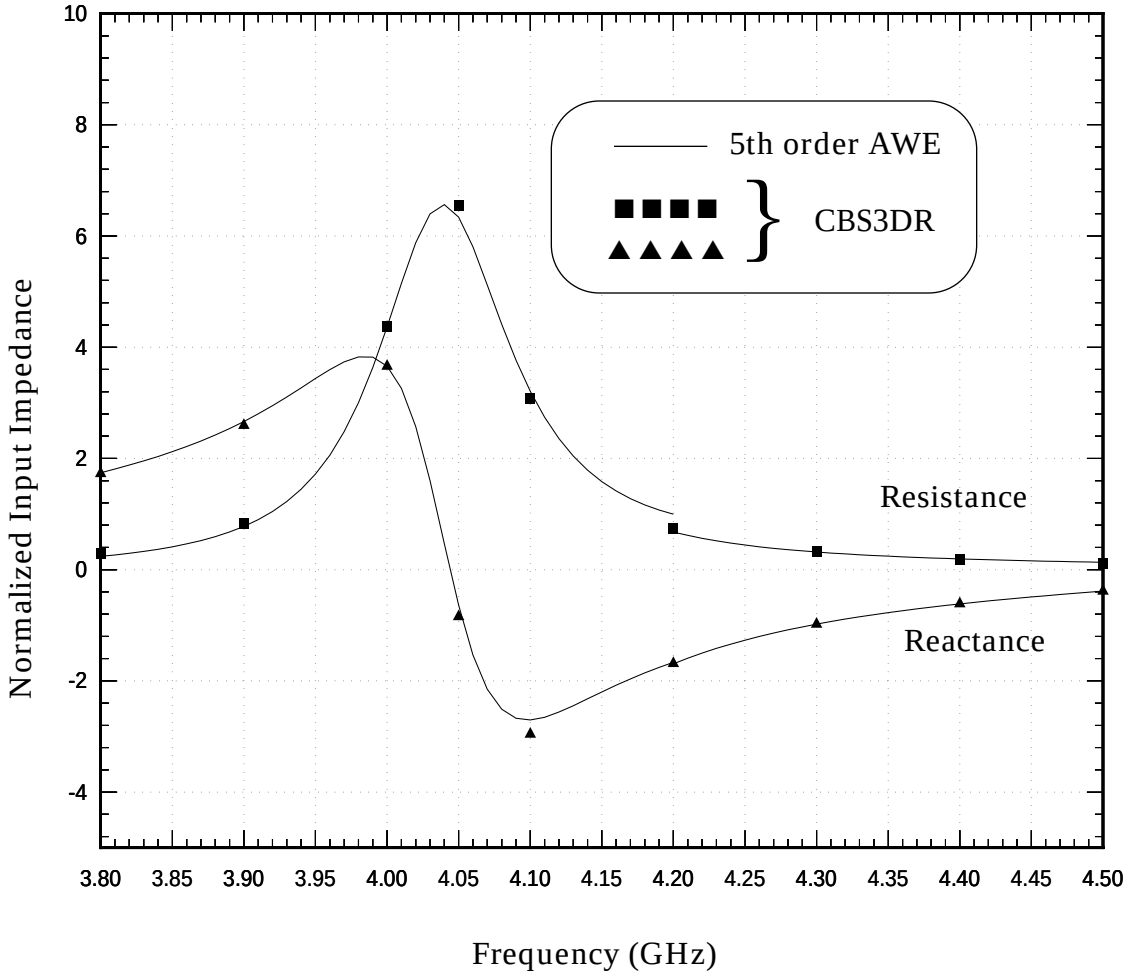

Figure 7 Normalized input impedance versus frequency of the cavity-backed square microstrip antenna (figure 6).

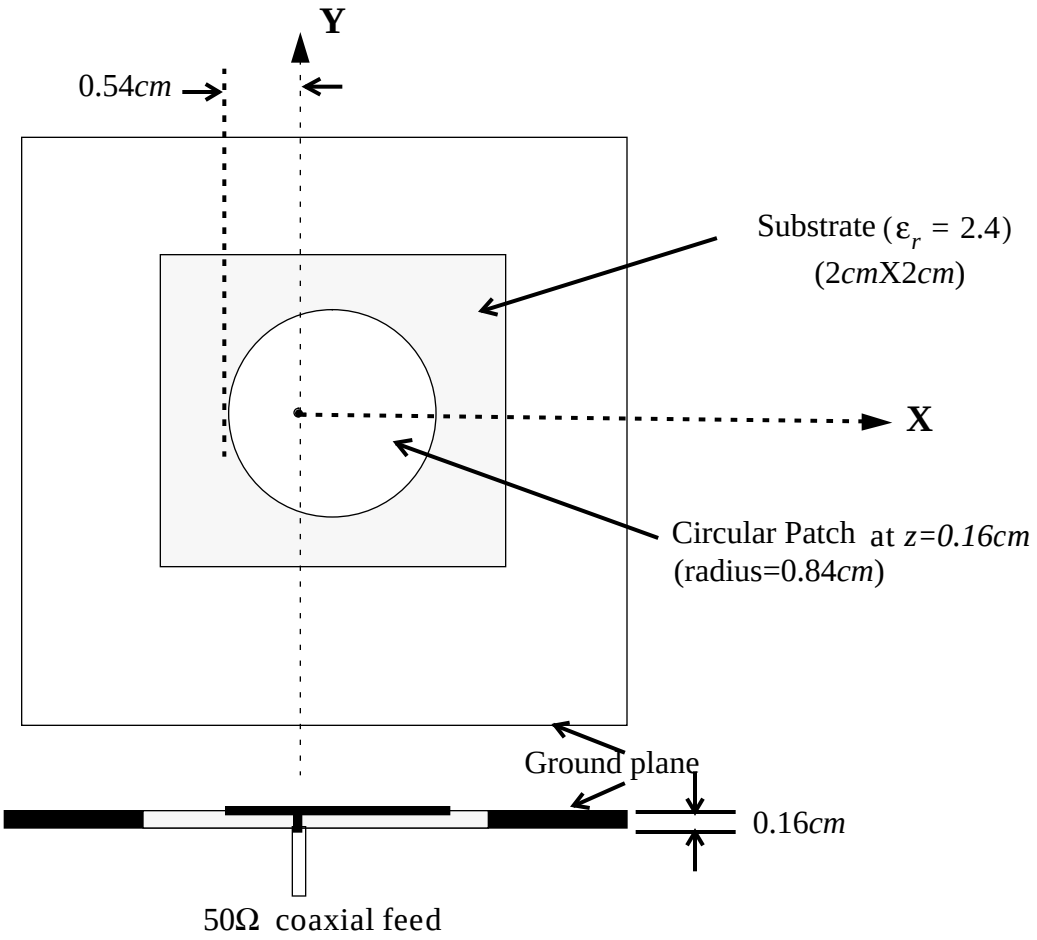

Figure 8 Cavity-backed circular microstrip patch antenna in an infinite ground plane fed by a 50Ω coaxial line.

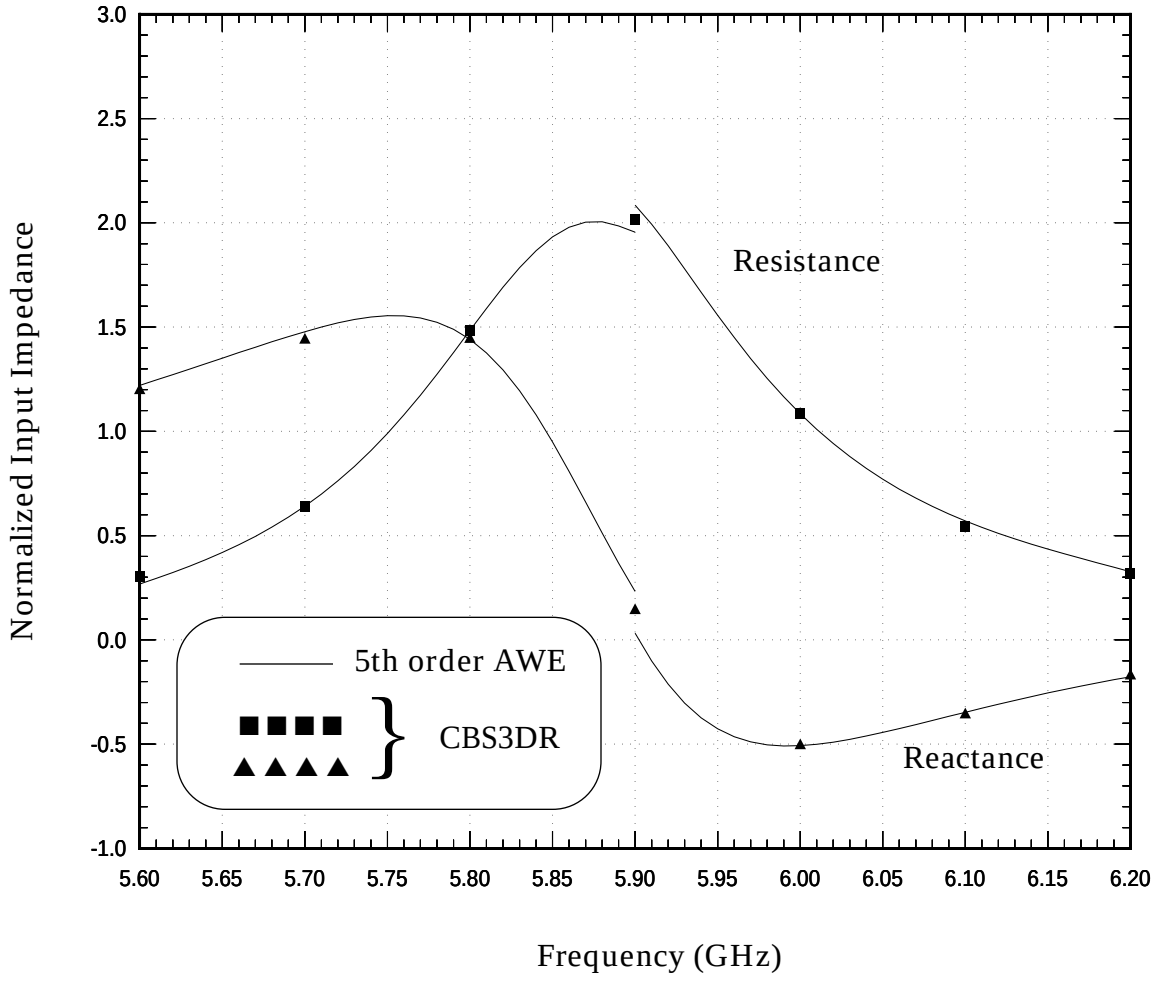

Figure 9 Normalized input impedance versus frequency of the cavity-backed circular microstrip antenna (figure 8).